Fabrication of a biobased hydrogel nanocomposite as a sustained drug delivery system

Highlights

In this chapter, starch/itaconic acid/acrylic acid-based hydrogel nanocomposite (HNC) was prepared by blending with gelatin in the presence of cellulose nanofiber/zinc oxide nanohybrid and used to evaluate the pH-sensitive *in vitro* drug release properties in different pH solutions. Moreover, pH-responsive swelling behavior was also studied for the prepared HNC. Further, the antibacterial property of the drug-encapsulated HNC was investigated against the gram-positive and gram-negative bacterial strains. A hemolysis test was also performed to study the hemocompatibility of the prepared nanocomposite. Thus, the results indicate that the prepared HNC can be used as a promising drug delivery system.

Parts of this chapter are published as

[1] Bora, A., Sarmah, D., Rather, M.A., Mandal, M., and Karak, N. Starch, gelatin and itaconic acid-based biodegradable hydrogel nanocomposites with ZnO/cellulose nanofiber as a pH-sensitive sustained drug delivery vehicle. *International Journal of Biological Macromolecules,* 256(1):128253, 2023.

6.1. Introduction

As explained in **Chapter 1,** great efforts have been made for research in the biomedical field for the development of an effective sustained drug delivery system (DDS). This is because conventional drug delivery such as tablets, ointments, capsules, etc. requires repetitive administration of an active compound to maintain the therapeutics levels in the human body which affects patient compliance and effectiveness and can lead to high-dose drug-related side effects [1]. Moreover, poor retention and low bioavailability are the limitations observed in the case of conventional DDS [2]. Therefore, polysaccharides and proteins-based hydrogel nanocomposites (HNCs) have been widely used as an emerging DDS for the sustained release of drugs in recent years. Besides their biocompatibility, biodegradability and cost-effective nature, they possess excellent drug-encapsulation efficiency (EE), stimuli-responsive, less severe side effects and slow drug release properties which greatly improve the convenience and effectiveness of drug delivery [3]. As described in **Chapter 1,** HNCs have been developed by incorporation of various organic or inorganic nanomaterials (NMs) through different mechanisms. They can absorb significant amounts of water or other biological fluids within their network structures and provide an environment similar to soft tissues [4]. Moreover, HNCs possess enhanced water swelling and drug loading capacity, decreased burst-drug release effect, improved drug stability, maintained slow and continuous drug release profiles, etc. compared with the bare hydrogel matrix [5,6]. As discussed in **Chapter 5,** among various inorganic metal and metal oxide NMs, zinc oxide (ZO) nanoparticles (NPs) have attracted significant attention from many researchers due to their favorable properties such as non-toxic, antibacterial, low production cost, high stability, etc. Therefore, ZO NPs have been considered as promising NM for biomedical applications. Further, ZO NPs can be obtained easily through a biogenic route by the utilization of eco-friendly and non-toxic approaches [7]. Besides, cellulosic NMs including cellulose nanofibers (CNFs), cellulose nanocrystals (CNCs), and cellulose nanowishkers (CNWs) are frequently used for drug delivery applications due to their sustainable, specific surface area, biocompatible, recyclable, biodegradable, modifiable, and low-cost nature [8]. Therefore, the fabrication of nanohybrid based on cellulosic NMs decorated with metal oxide NPs is considered as one of the most fascinating and rapidly emerging fields of material chemistry study as it synergistically enhances the performance of the resulting

material. Moreover, the utilization of cellulosic NMs also prevents metal NPs from aggregation.

Based on the above considerations, starch/gelatin/itaconic acid (IA)/ acrylic acid (AA)-based HNCs with the incorporation of CNF/ZO nanohybrid (ZONH) were fabricated and ciprofloxacin (CFX) was encapsulated into the matrix via an *in-situ* approach. In this work, gelatin was used as a bio-based material, besides using starch and IA because it contains a large number of functional groups that provide opportunities for cross-linking and to bind with the targeting ligand, which makes it extremely useful for developing DDSs [8]. Additionally, CFX was used as a model drug as it is the most commonly used antibiotic in the treatment of diverticulitis and various kinds of bacterial infections caused by both gram-positive and gram-negative pathogens [9]. Moreover, the EE (%) and pH-responsive *in-vitro* release performance of the prepared drug-encapsulated HNCs were investigated. The prepared HNCs were characterized by various instrumental techniques. The drug-encapsulated HNC was further used to investigate antibacterial activity against *Escherichia coli* (EC) and *Staphylococcus aureus* (SA) bacterial strains. Besides, a water swelling test was carried out in different pH media to investigate the pH-responsive swelling behavior of HNCs. To judge the biocompatibility of the HNC, a hemolysis test was also carried out.

6.2. Experimental section

6.2.1. Materials

Various chemicals including starch, AA, IA, N,N'-methylene bis-acrylamide (MBA), and ammonium persulfate (APS) were used with similar quality and specifications as mentioned in **Chapter 2.**

CFX was used as the model drug in this work and was supplied by SRL, India. It has a molar mass of 331.34 g/mol and is soluble in water.

The nanohybrid based on CNF and ZO was used as a reinforcing agent and was obtained by using the same procedure as mentioned in **Chapter 5**.

Luria-Bertani agar (LB) media was obtained from Himedia, India and used in an antibacterial test.

EC and SA bacterial strains were purchased from MTCC Chandigarh, India and used for antibacterial test.

6.2.2. Methods

6.2.2.1. Fabrication of hydrogel nanocomposites (HNCs)

The ZONH incorporated starch/gelatin/IA/AA-based HNCs were fabricated by using a similar method as described in **Chapter 5** with some modifications. First, desired amount of starch and IA were mixed in a three-neck round-bottom flask containing 10 mL of NaOH (0.067 N) solution with stirring at 80 °C. When the mixture became gelatinized, the temperature of the reaction was decreased to 60 °C and the solution of AA with 1 mL of water was then added to the mixture. After 10 min of stirring, MBA and the desired volume of ZONH dispersion were added and stirred for complete mixing. The mixture was then allowed to undergo polymerization by adding APS under a nitrogen environment. When the gel started to form, gelatin dissolved in 3 mL of water was added to the mixture and after the complete formation of the hydrogel, the reaction was cooled down to room temperature, washed with methanol and dried in an oven and then ground into a powder. For comparison, a bare hydrogel (without ZONH) was also synthesized by the same method as described above.

6.2.2.2. Synthesis of *in situ* drug encapsulated HNCs

Drug (CFX) encapsulated HNCs were prepared according to the above-described procedure. Additionally, CFX (0.025 g) was dissolved together with gelatin in 3 mL of water and added to the mixture when the gel was started to form. In **Table 6.1**, compositions of the prepared HNCs are provided.

Table 6.1. Composition of HNCs.

Hydrogel	Starch (g)	Gelatin (g)	IA (g)	AA (g)	ZONH (wt%)	CFX (g)
SAIG-1	1	0.3	0.1	0.9	0	0
SAIG-2	1	0.3	0.1	0.9	0.25	0
SAIG-3	1	0.3	0.1	0.9	0	0.025
SAIG-4	1	0.3	0.1	0.9	0.25	0.025

6.2.2.3. Structural analysis

Details of the instruments used for various analyses including Fourier transform infrared spectroscopy (FTIR), X-ray diffraction (XRD), field emission scanning electron microscopy (FESEM), and energy dispersive X-ray (EDX) were discussed in **Chapter 2, Chapter 3 and Chapter 4.** The elemental composition of the samples was carried out by X-ray photoelectron spectroscopy (XPS) (Model: ESCALAB 220 XL, UK). The details of UV-visible spectrophotometer used to study the sustained release of CFX from the

HNC were mentioned in **Chapter 2**. Optical density (OD) was determined for the hemolysis test using Thermo Scientific Multiscan GO spectrophotometer.

6.2.2.4. Water swelling test

The water absorption capacity (WAC) of the synthesized HNCs was measured using **Eq. 2.1** as mentioned in **Chapter 2**.

Further, the WAC of the prepared HNCs was tested at different pHs (4-9) to investigate the pH-responsive behavior of the HNCs.

6.2.2.5. Encapsulation efficiency (EE) measurement

In order to determine the EE, drug-encapsulated HNCs were washed with 50 mL of distilled water after the formation of the hydrogel product. Then, the amount of washed-out drug was determined by measuring the absorbance of the washout water using a UV-visible spectrophotometer at λ_{max} (270 nm) of the CFX. To follow this technique, 2 mL of washout solution was taken out and the absorbance of the aliquots was determined. To obtain the concentration of the washed-out drug from the absorbance value, a standard curve was prepared by utilizing known concentrations of CFX in water. Then, the percentage of EE (%) was calculated by using the following equation [10].

$$\text{EE (\%)} = \left(\frac{W_i - W_{wo}}{W_i}\right) \times 100 \text{ -------(Eq. 6.1)}$$

where W_i and W_{wo} are the initial amount of drug loaded within the hydrogel and the amount of drug washed-out from the hydrogel, respectively.

6.2.2.6. Drug release test

The *in vitro* drug release studies of the synthesized hydrogels were performed under physiological conditions (pH 7.4; phosphate buffer solution) and the concentration of drug released was calculated from absorbance measurement by following the same procedure as described in the previous section. Further, to comprehensively assess the pH-responsive behavior of the prepared hydrogels, we carried out the test in two other pH (4 and 9) solutions. The typical release experiment we adopted was as follows. To carry out the test, 0.5 g of the dried drug-loaded hydrogel was submerged in a beaker containing 50 mL of the test medium. After a predetermined time-interval, 1 mL of solution was removed and further diluted with 1 mL of water before measuring the

absorbance. In order to keep the volume of the testing medium constant, 1 mL of test solution was added to the beaker, immediately. Then, the percentage of drug-released was determined by using the following equation [11].

$$\text{Drug release (\%)} = \frac{M_t}{M_1} \times 100 \text{ --------(Eq. 6.2)}$$

where M_1 is the amount of drug remains inside the hydrogel after washing and M_t is the amount of drug released at time t.

6.2.2.7. Kinetic models of drug release

To understand the drug release mechanism and rate controlling processes for the drug release studies, obtained *in-vitro* drug-released data were applied in different models such as zero order, first order, Higuchi square root law and Korsmeyer–Peppas which were represented as **Eq. 3.1, Eq. 3.2, Eq. 3.3** and **Eq. 3.4** of **Chapter 3**.

6.2.2.8. Antibacterial performance test

The antibacterial activity of the prepared ZONH and CFX-loaded HNC (i.e., SAIG-4) against gram-positive (SA) and gram-negative (EC) bacterial strains was studied using a previously reported procedure [12]. The bacterial cultures viz., EC and SA were grown in LB media in an incubator at 37 °C for 16 h. The OD of the fresh culture was adjusted to 0.4 at 600 nm and used for the experiment. Further, each bacterial culture (100 µL) was spread evenly on the prepared LB plates. Then, ZONH, SAIG-4 and antibiotic solution (as positive control) were added to each plate, then incubated overnight at 37 °C. Finally, the antibacterial effect was investigated by measuring the diameter of bacterial growth inhibition.

6.2.2.9. Hemolysis assay

The hemolytic activity of SAIG-2 without CFX at different concentrations (0.25, 0.5, 0.75, 1, 5 and 10 mg/mL) was studied by following the protocol stated by Rather *et al.* with a slight modification [13]. Initially, an amount of defibrinated sheep blood was centrifuged at 4 °C to collect the pellets, which were washed with NaCl (0.9%) and centrifuged again. The washing step was performed two times, consecutively and finally, the pellets were suspended in NaCl (0.9%) solution. Then, samples of desired concentrations were prepared by adding RBC-suspended solution to different centrifuge

tubes and kept for 30 min at 37 °C and centrifuged again after incubation. Then, 200 µL of samples from each centrifuge tube was added into a 96-well plate and the OD was determined using Thermo Scientific Multiscan GO spectrophotometer at 540 nm to quantify cell lysis and hemoglobin release. Herein, water as well as Triton X-100 were used as the positive controls and NaCl (0.9%) was used as a negative control. The percent hemolysis was calculated by using the following equation.

$$\text{Hemolysis (\%)} = \frac{(A_S - A_{NC})}{A_{PC} - A_{NC}} \times 100 \text{ ---------(Eq. 6.3)}$$

where A_{PC}, A_{NC} and A_S are the absorbance of positive control (water), negative control and treated samples, respectively.

6.3. Results and discussion

6.3.1. Preparation of HNCs

The possible mechanism for the formation of ZONH-incorporated starch/gelatin/IA/AA-based HNC involves free radical polymerization in an aqueous medium [14]. In the initial step, APS undergoes thermal dissociation to produce sulfate radicals that abstract hydrogen from primary -OH groups of starch to form alkoxy macroradicals. Consequently, the macroradicals generate radical sites on AA and IA monomers. Thus,

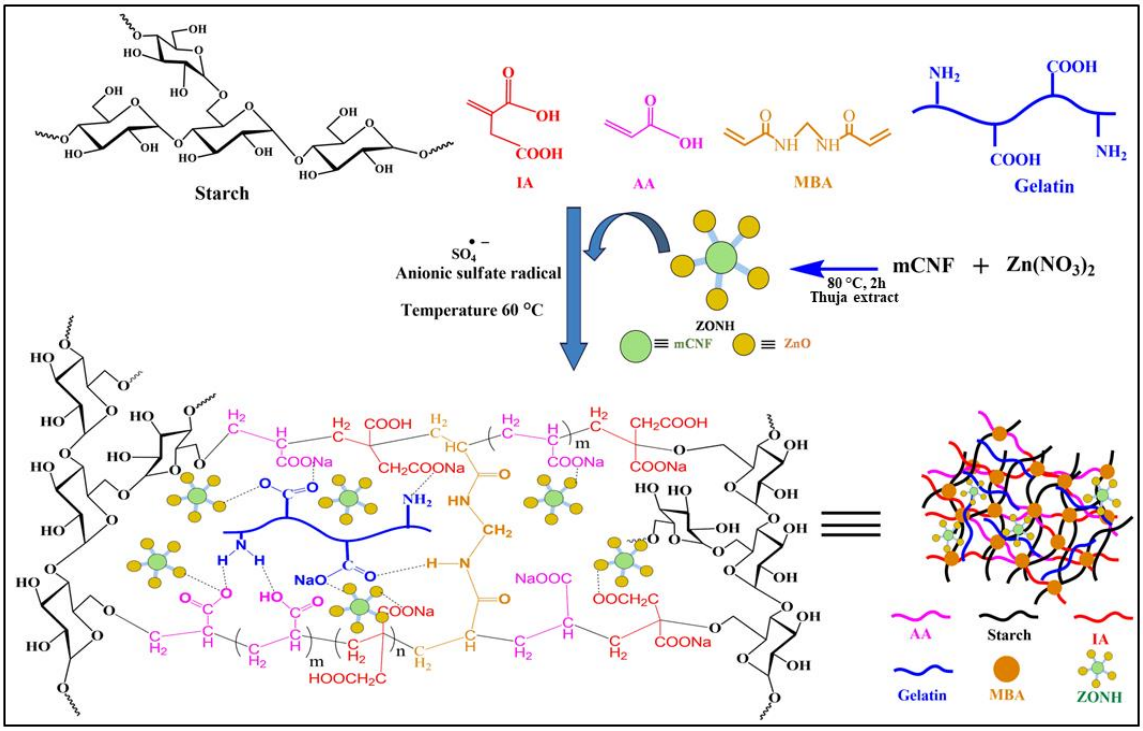

Scheme 6.1. Schematic representation of fabrication of the HNC.

the grafting of AA and IA takes place on the starch surface during the chain propagation step. Further, the two polymerizable vinyl groups of MBA bind simultaneously with the polymer chains to form a three-dimensional network structure. Moreover, in this work, gelatin was added during gelatinization, which is assumed to remain inside the hydrogel network via physical cross-linking, forming a semi-interpenetrating polymer network. The possible interactions of ZONH with the polymer matrixes are shown in **Scheme 6.1**, which clearly evident their strong compatibility in the HNC.

6.3.2. Characterization

6.3.2.1. FTIR

The FTIR spectra of SAIG-1 and SAIG-2 are shown in **Figure 6.1.a**. The peaks at 3498 and 2929 and 1017 cm^{-1} indicate the presence of O-H stretching, C-H asymmetric stretching, and C-O-C stretching, respectively, which are the characteristic peaks of starch [15]. The other peaks at around 1630 and 1720 cm^{-1} are observed in the case of both SAIG-1 and SAIG-2 spectra which can be ascribed to the C-O and C=O stretching vibration of carboxyl and amide groups of gelatin, AA and IA [10]. All these characteristic peaks together with a peak at 578 cm^{-1} for Zn-O bond were observed only in the case of SAIG-2, supporting the successful grafting of HNCs [16].

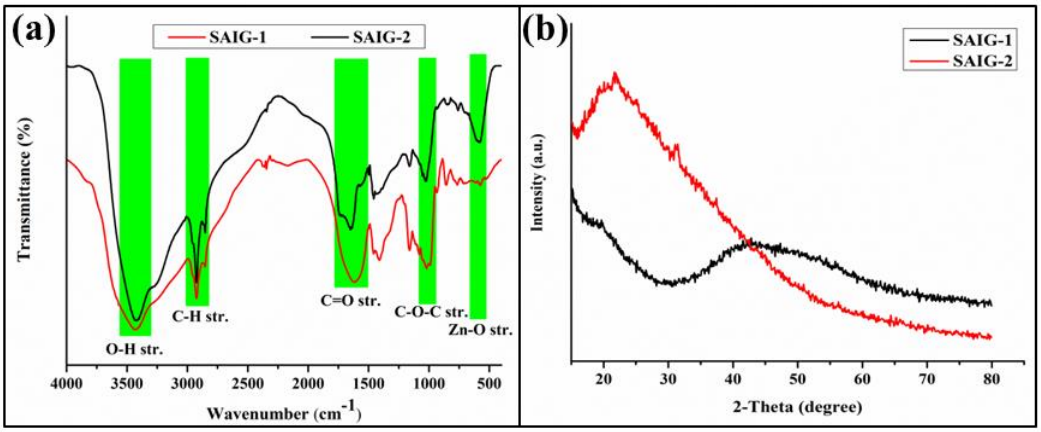

Figure 6.1. (a) FTIR spectra and (b) XRD patterns of SAIG-1 and SAIG-2.

6.3.2.2. XRD

The XRD analysis of SAIG-1 (without ZONH) and SAIG-2 (with ZONH) was carried out and the resulting patterns are shown in **Figure 6.1.b.** From this figure, two broad XRD peaks around 2θ values of 20° and 40° were observed for SAIG-1 representing the amorphous nature of the hydrogel matrix. As shown in **Chapter 5**, the characteristic XRD peaks for ZONH were observed at 22.23°, 31.56°, 34.11°, 36.02°, 47.29°, 56.11°,

62.56°, 66.04°, 67.79°, 68.91°, 72.09° and 76.70°. However, all of these characteristic peaks were not clearly observed in the XRD pattern of SAIG-2. Nevertheless, after ZONH loading, the intensity and width of the peak increased and a broader peak from 15 to 50° was observed in the case of SAIG-2 which indicated the presence of interaction between ZONH and the hydrogel matrix, affecting the crystal structure in the case of SAIG-2.

6.3.2.3. XPS

Consecutively, XPS analysis was performed to determine the chemical compositions and interactions present on the surface of both ZONH and SAIG-2. The complete spectrum of ZONH as shown in **Figure 6.2.a**, revealed the presence of 28.58% of zinc (Zn 2p), 44.73% of oxygen (O 1s) and 25.69% of carbon (C 1s) on the surface. In **Figure 6.2.(b-d)**, the high-resolution spectra of Zn 2p, O 1s and C 1s are shown. From the Zn 2p spectrum (**Figure 6.2.b**), the peaks corresponding to $Zn2p_{3/2}$ and $Zn2p_{1/2}$ were observed at 1021.11 and 1044.26 eV, respectively [17]. Further, three deconvoluted peaks were obtained in the O 1s spectrum (**Figure 6.2.c**), with different binding energies of 529.90, 531.42 and 532.66 eV which can be allocated to the Zn-O, Zn-O vacancy and O-C-O

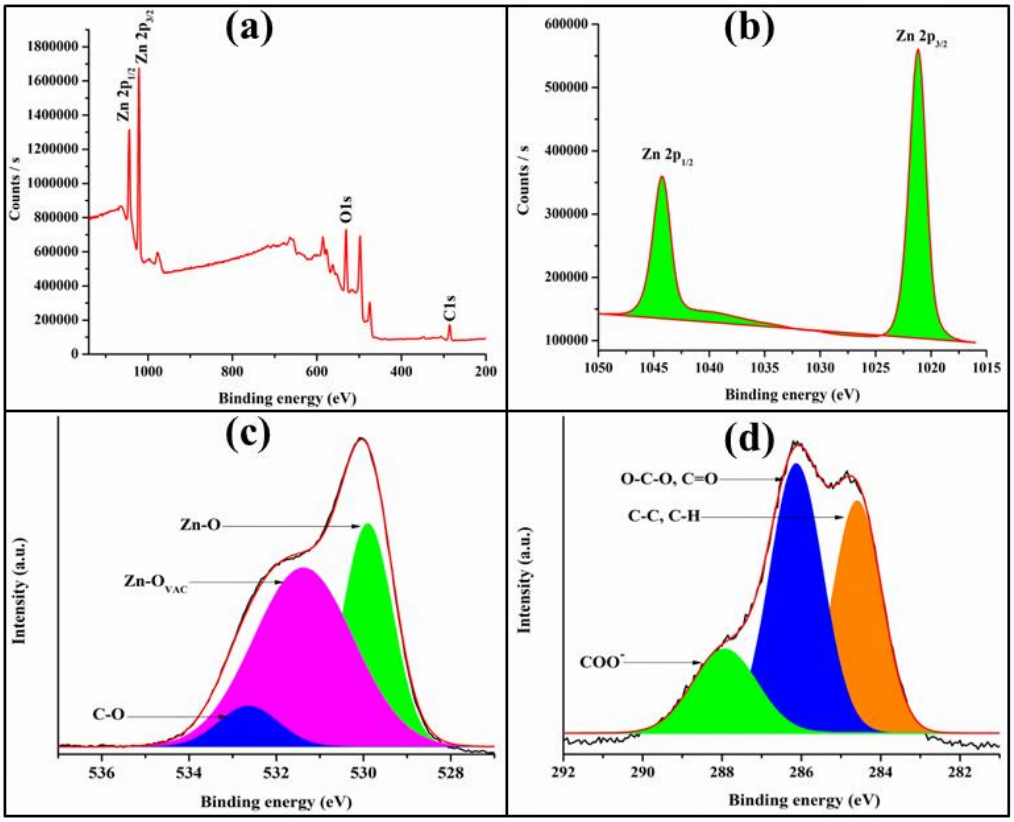

Figure 6.2. (a) XPS survey spectrum of ZONH. High-resolution XPS spectra of (b) Zn 2p region, (c) O 1s region and (d) C 1s region of ZONH.

bonding of oxygen present in the ZONH [18]. As shown in **Figure 6.2.d**, C 1s displayed three deconvoluted peaks of mCNF at 284.57, 286.15 and 288.06 eV which can be allocated to the C-C/C-H, C=O/O-C-O and O=C-O$^-$, respectively [19]. Thus, C 1s and O 1s spectra confirm the presence of mCNF in ZONH and these results also confirm the elemental composition of ZONH.

XPS analysis was further conducted to investigate the chemical constituents of the prepared hydrogel (SAIG-2). In **Figure 6.3.a**, full XPS spectrum of SAIG-2 is shown. The spectrum indicates that SAIG-2 contains 33.97% of O 1s, 0.8% of nitrogen (N 1s), 65.1% of C 1s and 0.13% of Zn 2p. From the C 1s spectrum (**Figure 6.3.b**), three deconvoluted peaks were observed at 284.79, 286.01 and 288.90 eV corresponding to C-C/C-H, O-C-O/C=O and O=C-O$^-$ bonding, respectively [19]. Further, high-resolution

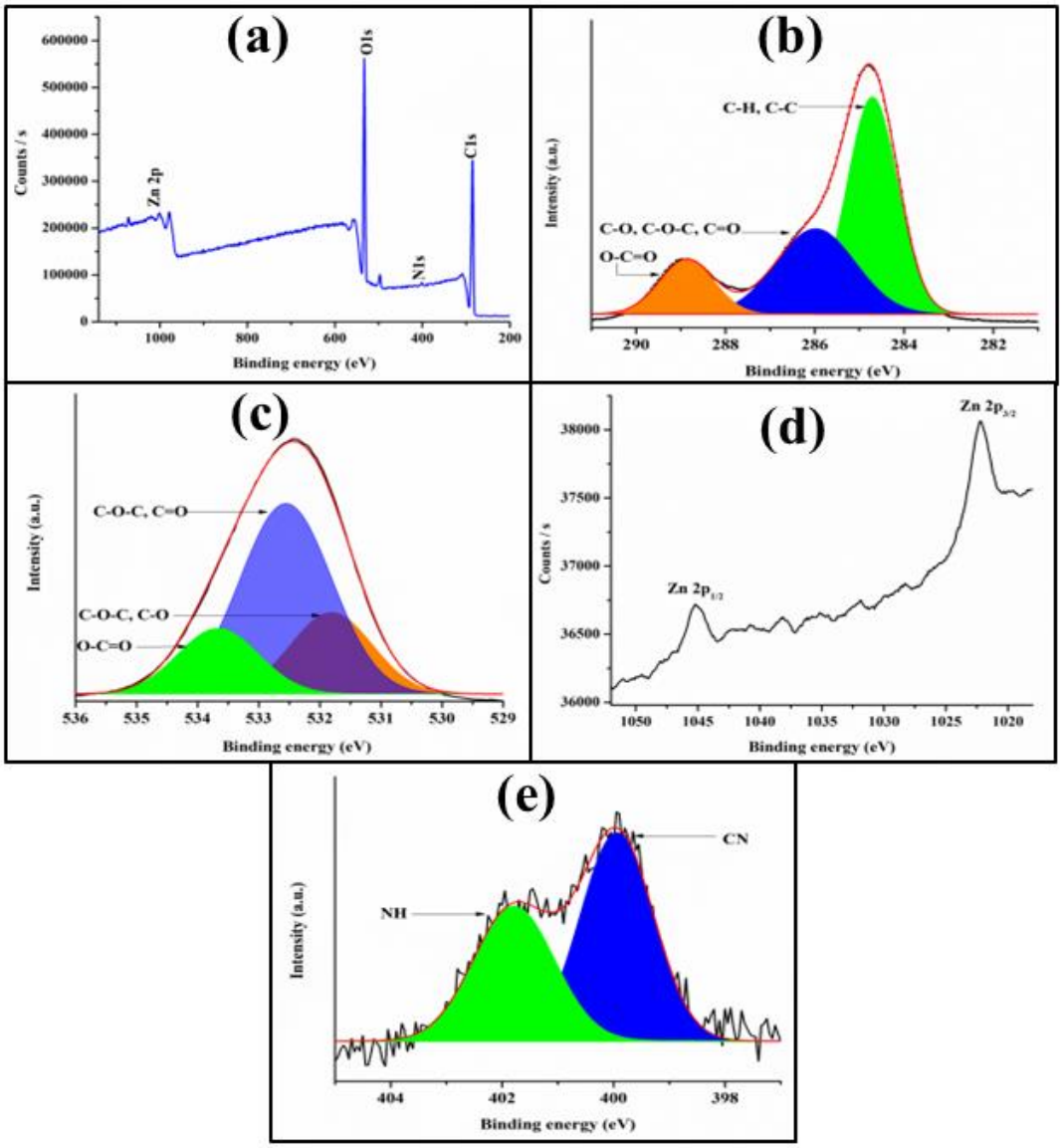

Figure 6.3. (a) XPS survey spectrum of SAIG-2. High-resolution XPS spectra of (b) C 1s region, (c) O 1s region, (d) Zn 2p region and (e) N 1s region of SAIG-2.

spectrum of O 1s (**Figure 6.3.c**) shows three deconvoluted peaks with binding energies at 531.79, 532.53 and 533.68 eV which can be allocated to C-O-C/C-O/Zn-O, C=O and O=C-O$^-$, respectively [20]. The Zn2p spectrum (**Figure 6.3.d**) of SAIG-2 shows two peaks with lower intensity at 1022.23 and 1045.22 eV, corresponding to $Zn2p_{3/2}$ and $Zn2p_{1/2}$, respectively [21].

Moreover, N 1s spectrum shows two peaks for CN and NH groups at 399.90 and 401.77 eV, respectively which can be attributed to the presence of MBA (**Figure 6.3.e**) [22]. Thus, from the XPS analysis together with FTIR and XRD results, we can confirm the successful preparation of ZONH-incorporated HNC via physical and chemical cross-linking.

6.3.2.3. EDX analysis

Further, EDX analysis was performed on the surface of SAIG-2. As can be seen in **Figure 6.4.a**, the EDX spectrum of SAIG-2 confirms the presence of ZONH on the surface. Moreover, a very nice ZONH distribution was observed from the EDX mapping analysis, as shown in **Figure 6.4.b.**

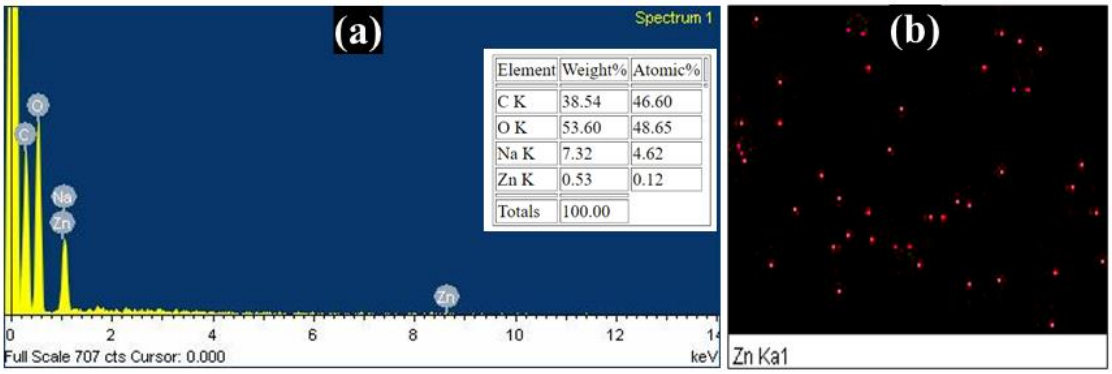

Figure 6.4. (a) The EDX spectrum of SAIG-2 and (b) EDX mapping image of ZONH distributed on SAIG-2 surface.

6.3.2.4. FESEM

The surface of a hydrogel is considered as one of the most significant factors affecting the swelling capacity and drug release rate to a large extent. In this study, the interfacial interactions between ZONH and the hydrogel matrix might have noticeable effects on the surface morphology as well as on the swelling capacity and drug release rate of SAIG-2 [23]. Therefore, morphological characteristics of the prepared HNC were investigated using the FESEM technique and the images are represented in **Figure 6.5**. From **Figure 6.5.a** at 2000X magnification, pores are observed on the surface of the HNC, indicating the formation of a three-dimensional network structure. Further, by

magnifying the surface up to 20,000X, we observed some pores with expected average diameter and lengths equal to or less than 1 µm **Figure 6.5.b**.

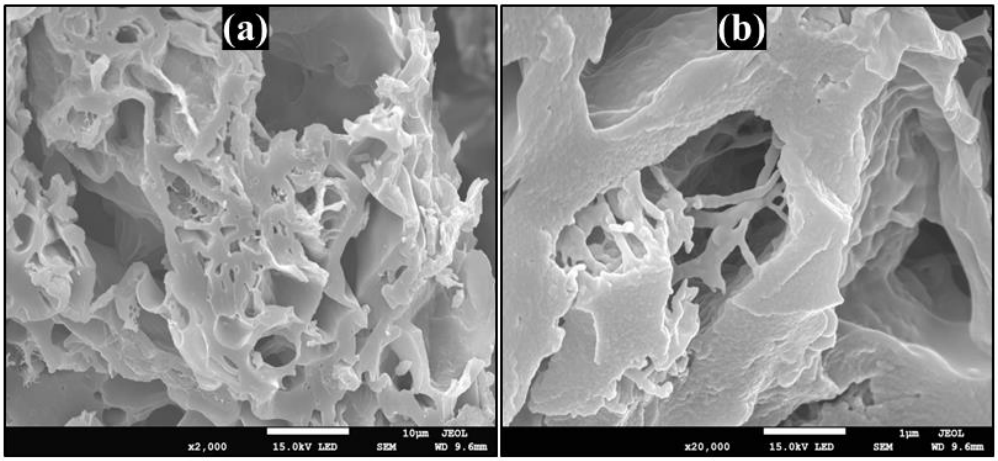

Figure 6.5. FESEM images of SAIG-2 at (a) 2000X (scale 10 µm) and (b) 20,000X (scale 1 µm) magnifications.

6.3.2.5. Water swelling study

Water absorbing property of hydrogel is an important factor from a biomedical point of view. Since hydrogel matrix comprises several hydrophilic groups, they may exhibit pH-responsive swelling behavior which assists in tuning the drug release property of the hydrogel. Therefore, the water absorption behavior of the synthesized hydrogels was determined in terms of different pH values of the swelling medium. Initially, WAC was investigated in distilled water to obtain the maximum WAC of the prepared hydrogels. As can be seen from **Figure 6.6.a**, both hydrogels possessed higher swelling capacity in water. However, an enhanced WAC was obtained in the case of SAIG-2 (332 g/g) compared to SAIG-1 (298 g/g). This observation can be ascribed to the effect of ZONH on the structure of SAIG-2, which could result in more pores and free spaces (due to its nanoscale dimension) within the hydrogel network structure [24]. Further, the presence of ZONH might introduce additional charged groups within the SAIG-2 network structure, which results in the diffusion of more water molecules to balance the generated ionic osmotic pressure, causing the hydrogel to swell more [6]. Similar results were also observed for starch and cellulose-based hydrogel in which water swelling capacity was increased due to the incorporation of ZnO NPs [24]. As the amounts of NPs increased, expansion of the hydrogel matrix occurred, causing penetration of water molecules to the network structure.

Further, the pH-sensitive swelling behavior of synthesized hydrogels was investigated at different pH conditions and the results are shown in **Figure 6.6.b**. These results indicate

that water absorbencies were found to be continuously increased for both samples with the increasing pH of the medium. At pH 4, most of the carboxylate groups present in the hydrogel may get protonated, which reduces the electrostatic repulsion or creates inter-molecular hydrogen bonds between them which in turn results in a lowering of WAC [9,25]. Moreover, a continuously increasing trend for water absorbency was obtained with the increasing pH of the medium, and the highest WAC of 369 g/g and 385 g/g for SAIG-1 and SAIG-2 was observed at pH 9, respectively. When the pH of the solution increases deprotonation of carboxylic acid groups occurs resulting in an increase in the electrostatic repulsion between them. Thus, diffusion of more water molecules takes place to balance the osmotic pressure gradient in the hydrogel [7].

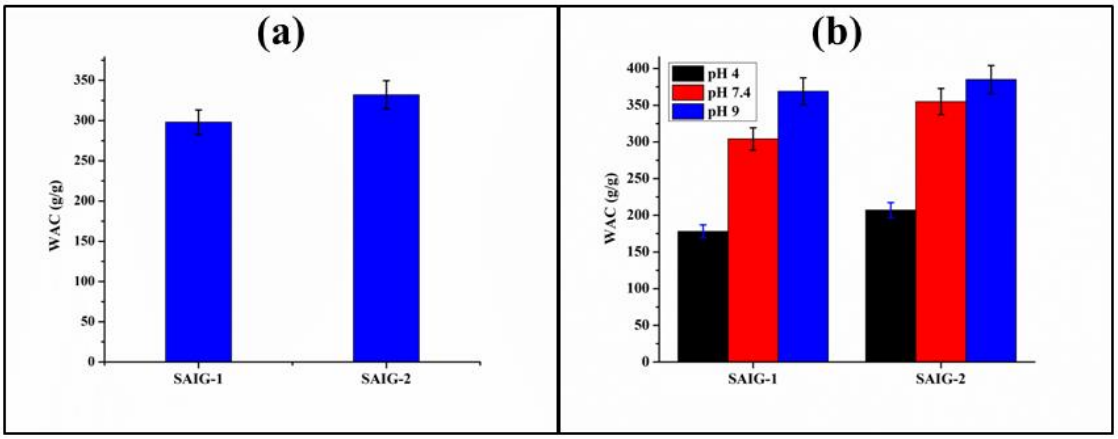

Figure 6.6. Water absorption capacity of SAIG-1 and SAIG-2 in (a) distilled water and (b) different pH values.

6.3.2.6. EE of drug-loaded HNCs

In this work, we used the *in-situ* approach to load CFX in the HNC because *in situ* loading approach is preferred over the post-loading one due to greater EE [26]. The percentage of EE is considered as an important parameter for the drug release system as it indicates the actual percentage of the drug present in the drug-encapsulated hydrogel. From **Figure 6.7.a**, it is observed that EEs for both hydrogels are >90%. The high EE observed for each HNC can be attributed to the presence of intermolecular interactions between CFX and the hydrogel matrix, and it indicates that the used hydrogel matrix is an effective carrier for CFX drug.

6.3.2.7. Drug release study

The stimuli-responsive property of a controlled DDS has a great effect on drug release because using this property, drug release rate and its targeted site can be tuned. As we

have already observed the pH-sensitive swelling ability of the prepared HNCs, so, CFX release study was investigated in different pH solutions to confirm the pH responsive properties of the prepared hydrogels. For comparison purposes, the test was conducted for both bare and nanocomposite hydrogels.

Initially, *in vitro* release of CFX from SAIG-3 and SAIG-4 was investigated at pH 7.4 and their corresponding release profiles were plotted as a function of time (**Figure 6.7.b**). From the figure, it was observed that SAIG-3 released 75% of encapsulated CFX in the first 5 h of incubation, while 41% of CFX was released from the SAIG-4 network for the same time period. The reason for the slow release of CFX from SAIG-4 compared to SAIG-3 can be attributed to the presence of ZONH within the hydrogel network. Since nanohybrid comprises a large surface-to-volume ratio, so it can make strong interactions (such as hydrogen bonding, electrostatic attraction, etc.) with drug molecules which in turn leads to the prolonged release of encapsulated drugs from the network structure [7,23]. Additionally, Zn atom of the nanohybrid can form a chelate with one carboxyl group and three amino groups of CFX molecule which in turn results in a sustained release of CFX from the HNC matrix [27].

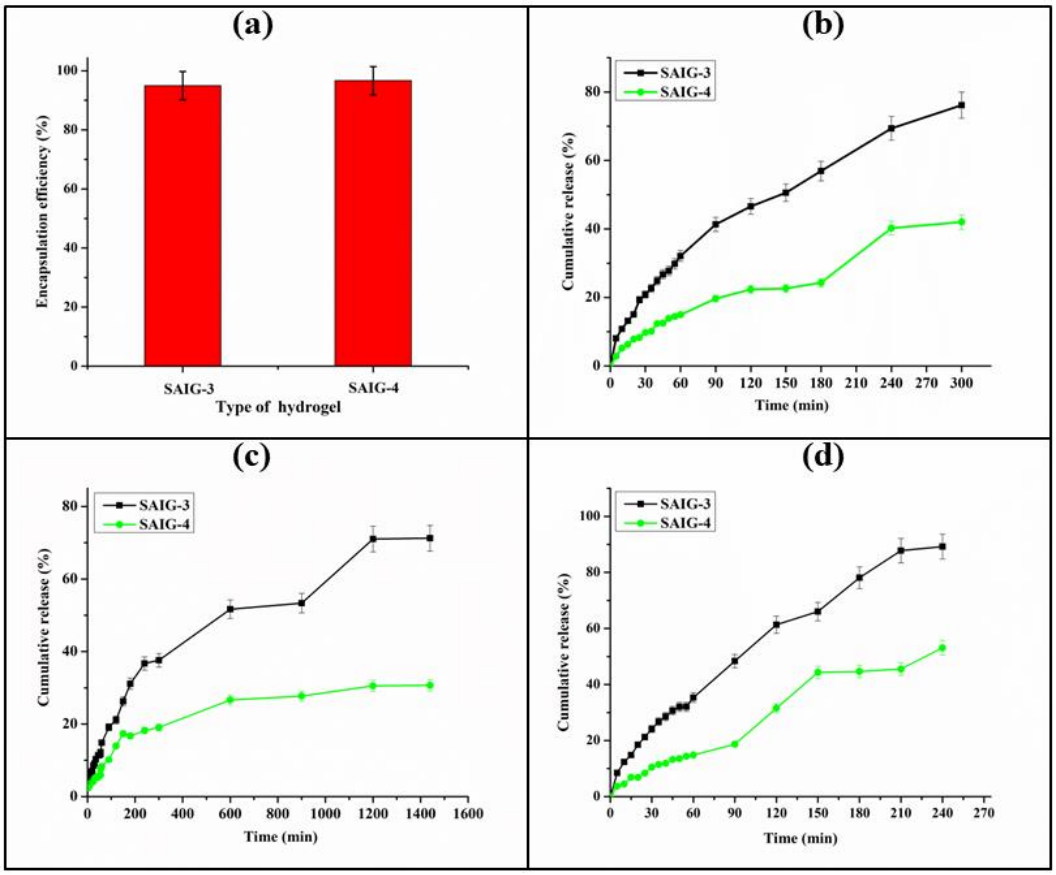

Figure 6.7. (a) Encapsulation efficiency of SAIG-3 and SAIG-4. Cumulative CFX release profiles of SAIG-3 and SAIG-4 at (b) pH 7.4, (c) pH 4 and (d) pH 9.

Further, the release of CFX from both hydrogels was carried out in pH 4 for 24 h and pH 9 for 4 h at room temperature, and the results are shown in **Figure 6.7.c** and **Figure 6.7.d**, respectively. As we can see in **Figure 6.7.c** that the release of CFX from SAIG-3 and SAIG-4 was found to be 70% and 30% in a 24 h studies, respectively. Whereas SAIG-3 released 88% and SAIG-4 released 52% of loaded CFX at pH 9, during the first 4 h of incubation. From these results, it was observed that the rate of CFX release from the HNCs at pH 9 was higher than at pH 4 and 7.4. Several explanations could have been given for this phenomenon. In acidic conditions, the carboxyl groups are protonated and form hydrogen bonding interactions between the chains, which in turn leads to a hydrophilic-hydrophobic phase transition, causing a sustained release of CFX from the HNCs [28]. Conversely at pH 9, carboxyl groups deprotonated and become hydrophilic in nature leading to the loosening of the hydrogel network structure resulting in more rapid drug delivery. Consequently, obtained results indicate that SAIG-4 releases CFX in a more sustainable manner and therefore, it can be more suitable as a pH-sensitive DDS for biomedical applications.

6.3.2.8. Kinetic study of drug release

To predict the CFX release mechanism of both SAIG-3 and SAIG-4 statistically, a kinetic study was carried out by using above-mentioned release models, and their corresponding plots are presented in **Figure 6.8**. Moreover, **Table 6.2** shows the highest correlation coefficient value for each hydrogel obtained in the case of Korsmeyer−Peppas model. Thus, this model has been considered to be the most suitable to study the release behavior of CFX from the prepared HNCs.

Table 6.2. Parameters for different kinetic models.

Hydrogel	Zero order	Pseudo first order	Higuchi Square root law	Korsmeyer -Peppas	n
SAIG-3	0.951	0.912	0.924	0.959	0.773
SAIG-4	0.968	0.970	0.943	0.970	0.740

In addition, the obtained ‘n’ value lies in the range of 0.45 to 0.89 which indicates that the release of CFX for both hydrogels following a non-Fickian transport mechanism

which typically takes place as a result of combined effects of diffusion and polymer chain relaxation [29].

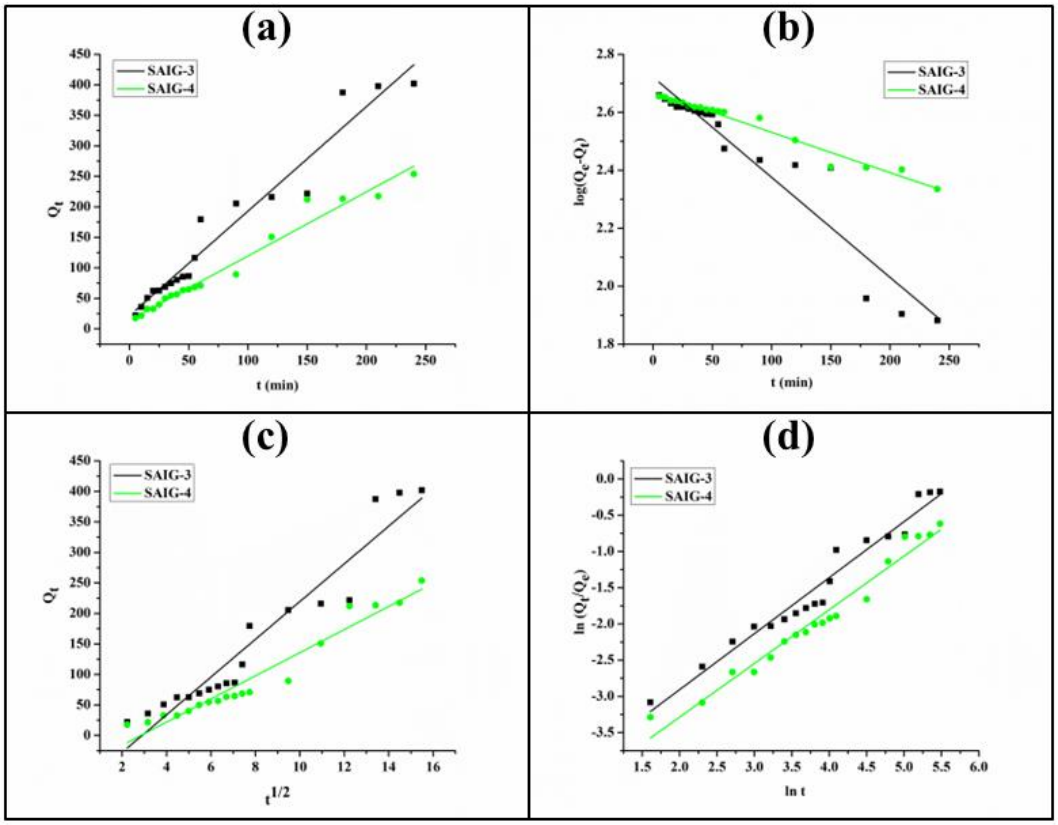

Figure 6.8. The plots of (a) Zero order, (b) Pseudo first order, (c) Higuchi square root law and (d) Korsmeyer and Peppas model for CFX released from SAIG-3 and SAIG-4.

6.3.2.9. Antibacterial test

CFX is a potent antibiotic belonging to second generation quinolone. It has great potential in the treatment of infections triggered by gram-negative and gram-positive bacteria [30]. To study antibacterial activity, CFX encapsulated hydrogel i.e., SAIG-4 was selected as the optimal formulation due to its pH-responsive slow-release property which makes this formulation desirable for drug delivery application. As can be seen from **Figure 6.9.a**, both ZONH and SAIG-4 have positive antibacterial effects against SA and EC. The antibacterial activity of ZONH can be assigned to the production of reactive oxygen species such as H_2O_2 from the surface of ZnO NPs [31]. Further, SAIG-4 exhibited an inhibition zone against the bacterial strains which can be ascribed to the synergistic effect of ZONH and antibiotic (CFX) on antibacterial activities which continued to be retained in the loaded hydrogel effectively. Thus, this result indicates that the prepared hydrogel can be applied to an antibacterial drug-release vehicle for biomedical application. Moreover, the antibacterial activity of SAIG-4 also confirmed

the successful encapsulation of the drug within the hydrogel matrix and its ability to release the same.

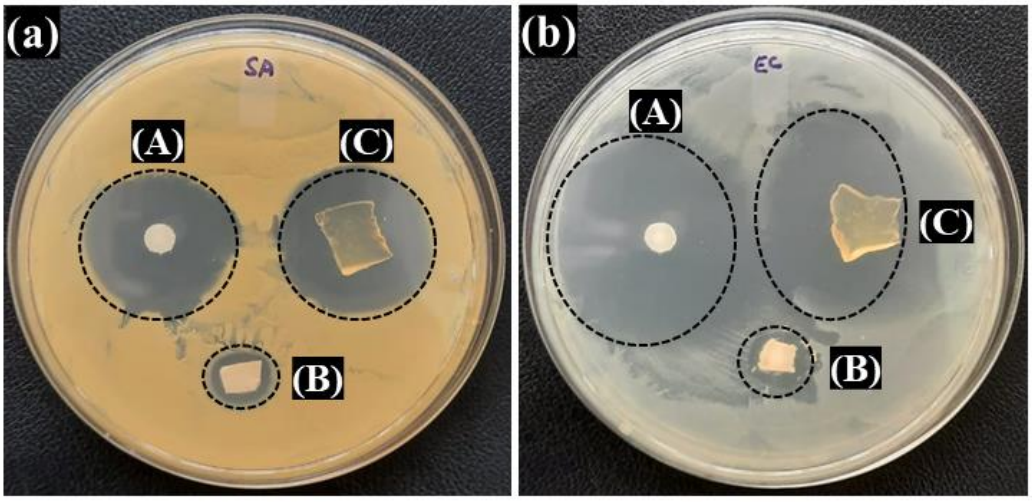

Figure 6.9. Digital photographs of LB plates showing inhibition zones of antibiotic solution (A), ZONH (B) and SAIG-4 (C) against (a) SA and (b) EC bacteria.

6.3.2.10. Hemolysis assay

The toxicity of polymeric materials is an important factor in their drug delivery applications [32**]**. The matrix itself must have no or a minimum level of toxicity to act as a safe drug carrier. Therefore, to investigate the biocompatibility of the prepared SAIG-2 without CFX encapsulation, a hemolysis test was carried out. The test investigates the destroying ability of a compound toward RBCs. For this, the test was carried out for different concentrations of SAIG-2 against defibrinated sheep blood, and the results are shown in **Figure 6.10.** and provided in **Table 6.3**. These results revealed that SAIG-2 exhibits significant biocompatibilities for all the concentrations of SAIG-2 except 10 mg/mL concentration, which showed hemolysis around 14%. Thus, within the scope of this work, SAIG-2 is found to have good biocompatibility and can be considered as a suitable material for drug delivery applications.

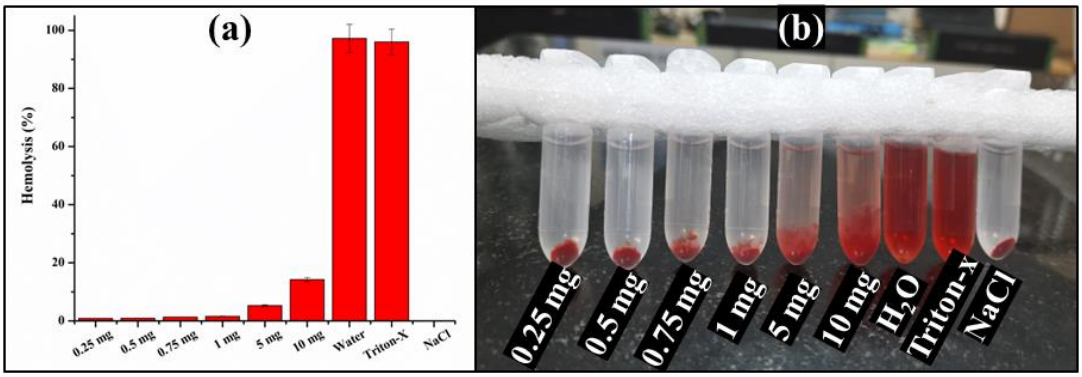

Figure 6.10. (a) Hemolysis percentage of SAIG-2 without encapsulation of CFX and (b) Digital photograph of RBCs treated with different concentrations of SAIG-2.

Table 6.3. Hemocompatibility results of SAIG-2 against sheep blood.

Sample	OD at 540 nm	Hemolysis (%)
0.25 mg	0.0713	0.864 ± 0.043
0.5 mg	0.0725	0.924 ± 0.066
0.75 mg	0.0805	1.324 ± 0.046
1 mg	0.0855	1.573 ± 0.710
5 mg	0.1600	5.295 ± 0.264
10 mg	0.3385	14.211 ± 0.078
Water	1.9999	97.198 ± 4.383
Triton-X	1.8091	87.667 ± 4.859
NaCl	0.0560	0.100 ± 0.005

6.4. Conclusion

In this study, ZnO/CNF loaded HNCs were prepared and characterized by different spectroscopic and microscopic analyses. CFX was successfully loaded and released from the hydrogel matrix. Since CFX was loaded via *in situ* approach, there was no difference in EE was observed for SAIG-3 and SAIG-4. The CFX release study indicates that the synthesized hydrogels exhibits pH-responsive behavior where it was observed that the hydrogels possess enhanced release rate when pH of the testing media changes from pH 4 to 9. Further, HNC loaded with nanohybrid possessed a slower release rate compared to bare hydrogel for each studied pH. Moreover, CFX release from both HNCs follows Korsmeyer-Peppas kinetic model with n values between 0.45 to 0.89 which indicates the release of CFX following the non-Fickian diffusion mechanism. The results of the antibacterial test indicate that the antibacterial activity for both nanohybrid and drug-loaded hydrogel can effectively inhibit the growth of gram-positive and gram-negative bacterial strains. The hemolysis test showed the biocompatibility of the prepared hydrogel. In conclusion, we can say that the prepared HNC can be used as a potential sustained DDS in biomedical applications.

References

[1] Santos, H. A. and Savina, I. N. Introduction to the RSC Advances themed collection on Nanomaterials in drug delivery. *RSC Advances*, 13(3):1933-1934, 2023.

[2] Singh Malik, D., Mital, N., and Kaur, G. Topical drug delivery systems: A patent review. *Expert Opinion on Therapeutic Patents*, 26(2):213-228, 2016.

[3] Zhao, J., Guo, B., and Ma, P. X. Injectable alginate microsphere/PLGA–PEG–PLGA composite hydrogels for sustained drug release. *RSC Advances*, 4(34):17736-17742, 2014.

[4] Dreiss, C. A. Hydrogel design strategies for drug delivery. *Current Opinion in Colloid and Interface Science*, 48:1-17, 2020.

[5] Lin, T., Zhang, J., Long, H., Yang, F., Huang, L., Deng, S. P., Zhang, J., Cai, X., Yang, Y., and Tan, S. Temperature-sensitive hydrogels containing carboxylated chitosan-modified carbon nanotubes for controlled drug release. *ACS Applied Nano Materials*, 5(8):10409-10420, 2022.

[6] Zare-Akbari, Z., Farhadnejad, H., Furughi-Nia, B., Abedin, S., Yadollahi, M., and Khorsand-Ghayeni, M. pH-sensitive bionanocomposite hydrogel beads based on carboxymethyl cellulose/ZnO nanoparticle as drug carrier. *International Journal of Biological Macromolecules*, 93:1317-1327, 2016.

[7] George, D., Maheswari, P. U., and Begum, K. M. S. Cysteine conjugated chitosan-based green nanohybrid hydrogel embedded with zinc oxide nanoparticles towards enhanced therapeutic potential of naringenin. *Reactive and Functional Polymers*, 148:104480, 2020.

[8] Li, J., Wang, Y., Zhang, L., Xu, Z., Dai, H., and Wu, W. Nanocellulose/gelatin composite cryogels for controlled drug release, *ACS Sustainable Chemistry and Engineering*, 7:6381-6389, 2019.

[9] Prusty, K. and Swain, S. K. Release of ciprofloxacin drugs by nano gold embedded cellulose grafted polyacrylamide hybrid nanocomposite hydrogels. *International Journal of Biological Macromolecules*, 126:765-775, 2019.

[10] Bhattacharyya, S. K., Dule, M., Paul, R., Dash, J., Anas, M., Mandal, T. K., Das, P., Das, N. C., and Banerjee, S. Carbon dot cross-linked gelatin nanocomposite hydrogel for pH-sensing and pH-responsive drug delivery, *ACS Biomaterials Science and Engineering*, 6:5662-5674, 2020.

[11] Luo, J., Ma, Z., Yang, F., Wu, T., Wen, S., Zhang, J., Huang, L., Deng, S., and Tan, S. Fabrication of laponite-reinforced dextran-based hydrogels for NIR-

responsive controlled drug release. *ACS Biomaterials Science and Engineering*, 8(4):1554-1565, 2022.

[12] Rather, M. A., Gupta, K., Gupta, A. K., Mishra, P., Qureshi, A., Dutta, T. K., Joardar, S. N., and Mandal, M. Phytochemical analysis and demonstration of antioxidant, antibacterial, and antibiofilm activities of ethnomedicinal plants of north east India. *Applied Biochemistry and Biotechnology*, 195(5):3257-3294, 2023.

[13] Rather, M. A., Deori, P. J., Gupta, K., Daimary, N., Deka, D., Qureshi, A., Dutta, T. K., Joardar, S. N., and Mandal, M. Ecofriendly phytofabrication of silver nanoparticles using aqueous extract of *Cuphea carthagenensis* and their antioxidant potential and antibacterial activity against clinically important human pathogens. *Chemosphere*, 300:134497, 2022.

[14] Sethi, S., Saruchi, Medha, Thakur, S., Kaith, B. S., Sharma, N., Ansar, S., Pandey, S., and Kuma, V. Biopolymer starch-gelatin embedded with silver nanoparticle–based hydrogel composites for antibacterial application. *Biomass Conversion and Biorefinery*, 12(11):5363-5384, 2022.

[15] Wang, Z., Shi, H., Wang, F., Wang, A., He, Q., and Cuan, S. Synthesis of cassava starch-g-acrylic acid/dimethylaminopropyl methacrylamide: A new hydrogel for brine solution. *Carbohydrate Polymers*, 266:118109, 2021.

[16] Quadri, T. W., Olasunkanmi, L. O., Fayemi, O. E., Solomon, M. M., and Ebenso, E. E. Zinc oxide nanocomposites of selected polymers: Synthesis, characterization, and corrosion inhibition studies on mild steel in HCl solution. *ACS Omega*, 2(11):8421-8437, 2017.

[17] Chee, W. K., Lim, H. N., Zainal, Z., Harrison, I., Huang, N. M., Andou, Y., Chong, K. F., and Pandikumar, A. Electrospun nanofiber membranes as ultrathin flexible supercapacitors. *RSC Advances*, 7(20):12033-12040, 2017.

[18] Cho, S. K. and Cho, W. J. Microwave-assisted calcination of electrospun indium–gallium–zinc oxide nanofibers for high-performance field-effect transistors. *RSC Advances*, 10(63):38351-38356, 2020.

[19] Rabani, I., Yoo, J., Bathula, C., Hussain, S., and Seo, Y. S. The role of uniformly distributed ZnO nanoparticles on cellulose nanofibers in flexible solid state symmetric supercapacitors. *Journal of Materials Chemistry A*, 9(19):11580-11594, 2021.

[20] Perumal, S., Atchudan, R., Yoon, D. H., Joo, J., and Cheong, I. W. Spherical chitosan/gelatin hydrogel particles for removal of multiple heavy metal ions from wastewater. *Industrial and Engineering Chemistry Research*, 58(23):9900-9907, 2019.

[21] Sekar, A. and Yadav, R. Green fabrication of zinc oxide supported carbon dots for visible light-responsive photocatalytic decolourization of Malachite Green dye: Optimization and kinetic studies. *Optik*, 242:167311, 2021.

[22] Heydari, N., Bikas, R., Shaterian, M., and Lis, T. Green solvent free epoxidation of olefins by a heterogenised hydrazone-dioxidotungsten(VI) coordination compound. *RSC Advances*, 12(8):4813-4827, 2022.

[23] Hossieni-Aghdam, S. J., Foroughi-Nia, B., Zare-Akbari, Z., Mojarad-Jabali, S., and Farhadnejad, H. Facile fabrication and characterization of a novel oral pH-sensitive drug delivery system based on CMC hydrogel and HNT-AT nanohybrid. *International Journal of Biological Macromolecules*, 107:2436-2449, 2018.

[24] Gholamali, I. and Yadollahi, M. Doxorubicin-loaded carboxymethyl cellulose/Starch/ZnO nanocomposite hydrogel beads as an anticancer drug carrier agent. *International Journal of Biological Macromolecules*, 160:724-735, 2020.

[25] Mahdavinia, G.R., Ettehadi, S., Amini, M., and Sabzi, M. Synthesis and characterization of hydroxypropyl methylcellulose-g-poly (acrylamide)/LAPONITE® RD nanocomposites as novel magnetic-and pH-sensitive carriers for controlled drug release. *RSC Advances*, 5(55):44516-44523, 2015.

[26] Guilherme, M. R., Aouada, F. A., Fajardo, A. R., Martins, A. F., Paulino, A. T., Davi, M. F., Rubira, A. F., and Muniz, E. C. Superabsorbent hydrogels based on polysaccharides for application in agriculture as soil conditioner and nutrient carrier: A review. *European Polymer Journal*, 72:365-385, 2015.

[27] Allahverdiyev, A. M., Kon, K. V., Abamor, E. S., Bagirova, M., and Rafailovich, M. Coping with antibiotic resistance: combining nanoparticles with antibiotics and other antimicrobial agents. *Expert Review of Anti-infective Therapy*, 9(11):1035-1052, 2011.

[28] Kanamala, M., Wilson, W. R., Yang, M., Palmer, B. D., and Wu, Z. Mechanisms and biomaterials in pH-responsive tumour targeted drug delivery: A review. *Biomaterials*, 85:152-167, 2016.

[29] Mao, Z., Li, J., Huang, W., Jiang, H., Zimba, B. L., Chen, L., Wan, J., and Wu, Q. Preparation of poly(lactic acid)/graphene oxide nanofiber membranes with different structures by electrospinning for drug delivery. *RSC Advances*, 8(30):16619-16625, 2018.

[30] Hanna, D. H. and Saad, G. R. Encapsulation of ciprofloxacin within modified xanthan gum-chitosan based hydrogel for drug delivery. *Bioorganic Chemistry*, 84:115-124, 2019.

[31] Yamamoto, O. Influence of particle size on the antibacterial activity of zinc oxide. *International Journal of Inorganic Materials*, 3(7):643-646, 2011.

[32] Sarmah, D., Rather, M. A., Sarkar, A., Mandal, M., Sankaranarayanan, K., and Karak, N. Self-cross-linked starch/chitosan hydrogel as a biocompatible vehicle for controlled release of drug. *International Journal of Biological Macromolecules*, 237:124206, 2023.